Observation of the Boson Peak in a 2D Material

Martin Tømterud[1,2*], Sabrina D. Eder[2], Christin Büchner[3], Lothar Wondraczek[4], Ingve Simonsen[1], Walter Schirmacher[5,6], Joseph R. Manson[7,8] and Bodil Holst[2*]

[1*]Department of Physics, NTNU–Norwegian University of Science and Technology, 7491 Trondheim, Norway.

[2*]Department of Physics and Technology, University of Bergen, Allégaten 55, 5007 Bergen, Norway.

[3]Fritz-Haber-Institut der Max-Planck-Gesellschaft, Faradayweg 4–6, 14195 Berlin Germany.

[4]Otto Schott Institute of Materials Research, University of Jena, Fraunhoferstrasse 6, 07743, Jena, Germany.

[5]Institute of Physics, University of Mainz, Staudinger Weg 7, 55099 Mainz, Germany.

[6]Center for Life Nano Science @Sapienza, Istituto Italiano di Tecnologia, 295 Viale Regina Elena I-00161 Roma, Italy.

[7]Department of Physics and Astronomy, Clemson University, Clemson, 29634, South Carolina, U.S.A..

[8]Donostia International Physics Center (DIPC), Paseo Manual de Lardizabal 4, 20018 Donostia-San Sebastían, Spain.

*Corresponding author(s). E-mail(s): martin.tomterud@uib.no; bodil.holst@uib.no;
Contributing authors: sabrina.eder@uib.no; cbuechner@lbl.gov;
lothar.wondraczek@uni-jena.de; ingve.simonsen@ntnu.no;
walter.schirmacher@uni-mainz.de; jmanson@clemson.edu;

Abstract

The boson peak is an excess in the phonon vibrational density of states relative to the Debye model. It has been observed in a wide range of amorphous materials, from inorganic glasses to polymers. 2D random matrix models and molecular dynamics simulations predict that the boson peak should also be present in amorphous 2D materials; a question which is of practical importance because it leads to an excess of heat capacity and influences transport properties. However, up until now, experimental observations in real-world materials have not been possible due to the limited surface sensitivity of the methods usually applied to measure the boson peak. Here we present experimental evidence of a boson peak in a 2D material obtained from 2D silica phonon spectra, measured with inelastic helium atom scattering. We identify the boson peak as a wavenumber-independent spectral maximum around 1.5 THz (6 meV), similar to what has been observed in and predicted for bulk vitreous silica. Furthermore, we present a heterogeneous-elastic theory calculation in 2D, which shows how the vibrational coupling of the transversal and flexural shear vertical (ZA) phonon modes produces the boson peak in 2D materials at a frequency similar to that of the bulk, in agreement with our measurements.

Keywords: boson peak, helium atom scattering, bilayer silica

Main

The Debye model predicts that below the Debye frequency, the vibrational density of states (VDoS) for a solid material is proportional to ω^{D-1}, where D is the dimensionality and ω is the the phonon frequency [1]. However, experiments have shown that many materials across the wide group of disordered materials exhibit a characteristic deviation from the Debye model prediction in the form of a broad, dispersionless excess of states relative to the expected frequency dependence. This deviation is commonly referred to as the *boson peak* (BP) [2–5]. The BP excess in the density of states is also found to be related to a similar excess in the heat capacity, $C(T)$, measured at low temperatures. There, the BP appears as a hump in $C(T)/T^3$ in the material bulk around 10 K [6, 7]. This hump in heat capacity is associated with an opposite effect on thermal conductivity. At the BP temperature, the thermal conductivity exhibits an upside-down BP [8], where the conductivity drops off in its temperature dependence. This thermal anomaly is also associated with the BP [9]. The BP has furthermore been observed to influence energy transport in amorphous materials, where coexisting diffusive and propagative energy transport has been observed in the BP frequency range [10].

The BP has been observed using a wide range of measurement techniques: Raman spectroscopy [2, 11–14], optical spectroscopy [15] including far-infrared spectroscopy [16, 17], X-rays [18], neutron scattering [19–21], and terahertz spectroscopy [22], as well as thermal techniques [23], including indirect verification through measurements of the temperature dependence of the heat capacity [8, 24]. A BP-like anomaly in the VDoS has also been observed in nanocrystalline ^{57}Fe [25], which is consistent with results of simulations of nanocrystals [26]. Due to their limited surface sensitivity, all of these experimental techniques address bulk material behaviour only; even grazing incidence X-ray [27] and grazing incidence neutron scattering [28] have penetration depths of a few nanometers, well above what one would consider the thickness of a 2D material.. Hence, the BP observed from such experiments reflects volumetric disorder. In 3D vitreous Silica the boson peak has been reported by inelastic neutron [19] and inelastic X-ray scattering [14] near the frequency of ~ 6 meV, whereby the X-ray boson peak has much less intensity than the neutron one [14].

In 2007, Steurer *et al.* presented the first observations of the BP as a surface phenomenon through measurements of phonon dispersion curves on vitreous silica obtained using inelastic helium atom scattering (HAS) [29–32]. HAS has a unique surface sensitivity. Unlike electrons, X-rays and neutrons, which all interact with the core electronic cloud and atomic nuclei in the sample, the neutral helium atoms scatter off the outermost charge density distribution at the sample surface with no penetration into the bulk. The classical turning point for helium atoms scattering at thermal energies is a few Ångströms above the surface [33]. HAS is therefore particularly suited for this type of measurement [34].

The BP has been observed in 2D macroscopic model systems consisting of colloid particles [35] and photo-elastic disks [36, 37] and it was recently claimed to have been observed in ultrathin alumina layers on oxidized aluminum nanoparticles [38], but up till now, it has not been experimentally observed in an atomically thin 2D material.

Theoretically, one has long assumed some form of disorder in a material to be a prerequisite for the existence of the BP as a bulk phenomenon. Early approaches used soft potentials and double-well potentials introduced into the Hamiltonian [39–42]. The VDoS for vitreous silica has been calculated using molecular dynamics simulations, leading to a prediction of the BP at around 6 meV [43] and around 7 meV [44], in good agreement with experimental Raman scattering data [2]. Molecular dynamics simulations have also been used by Wang *et al.* to calculate the BP at the surface of vitreous silica [45]. They obtained a BP at around 4 meV, in good agreement with the experimental HAS data mentioned above [29].

In 2004 [46] and later [9, 47] it was shown that the origin of the BP in bulk glass can be explained in the framework of heterogeneous-elasticity theory (HET). In particular, the anomalies of the specific heat and the thermal conductivity in the ~ 10 K region were shown to have the same origin as the BP, namely spatially fluctuating elastic constants.

At the same time, it was made clear by extensive simulations that the BP-related vibrational

anomalies of glasses are associated with non-affine displacement fields [48–52]. The non-affine aspects of the disorder-induced vibrational anomalies were shown to be accounted for by HET [47, 53]. Further, the BP frequency was shown to coincide with the Ioffe-Regel limit for the existence of plane-wave-like states [47, 54–56]. The states near and above the BP frequency were identified to be of random-matrix type [55, 57, 58].

The BP has been predicted theoretically to exist in 2D materials by molecular-dynamics simulations [54] and random matrix models [59–61]. In a recent review of modern silicate glasses, the BP frequency was reported using HET to vary between $4-6$ meV [53].

In the method section of this paper, we present a hitherto unpublished 2D HET calculation, which shows that the boson peak from elastic in-plane vibrations of a 2D material is coupled via disorder to the out-of-plane flexural shear vertical mode, also referred to as the ZA mode. This coupling arises via the disorder-induced frequency dependence of the effective flexural stiffness.

In this paper, we present the first experimental observations of the BP in a 2D material: amorphous 2D silica supported on Ru(0001). This 2D film system has generated considerable interest because it is a transferable, wide-bandgap material. The 2D silica film is weakly bound to the Ru(0001) substrate and can be peeled off [62, 63]. The silica bilayer is the thinnest arrangement of SiO_2 known [63], and, as it can be prepared in an amorphous phase, it has also been named the world's thinnest glass. The material is, therefore, of interest to the glass science community as it provides the opportunity to study a glassy 2D film and investigate experimentally how dimensionality impacts glassy properties. TEM imaging has been applied to confirm the 2D nature of the material [64] and to study atomic rearrangement in the glass [65]. It was shown in Ref. 66 that the mechanical properties of free 2D silica can be extracted from the phonon frequency spectrum. As discussed in Ref. 66, the phonon spectrum exhibits no prominent features (except the appearance of a gap in the dispersion of the ZA mode) that can be directly related to the underlying substrate. Therefore this 2D film system provides an excellent framework for investigating the BP using HAS and comparing it to the aforementioned earlier surface and bulk measurements. Because the BP is a disorder-induced phenomenon, the knowledge about this anomaly – and the corresponding modifications of the phonon spectrum – may be used for tuning the thermal properties of SiO_2 layers for applications [63]. Using inelastic HAS, we have obtained time-of-flight (TOF) spectra that provide the basis of our experimental analysis. The experimental setup and method are described in the Methods section. Examples of TOF spectra are shown converted to energy transfer ΔE in Fig. 1. These examples were chosen to cover the complete range of incident polar angles explored. The peak at $\Delta E = 0$ corresponds to diffuse elastic scattering, with no energy transfer with the surface. Negative values of ΔE correspond to phonon creation, positive values to phonon annihilation. The upward-pointing arrows indicate the ZA mode, which was analyzed in detail in Ref. 66 and used to obtain the bending rigidity of 2D silica. The downward-pointing arrows indicate the BP.

The TOF spectra, once they are converted to energy transfer, are known as the differential reflection coefficient (DRC) $dR/d\Omega dE$: the number of helium atoms dR scattered within a small solid angle $d\Omega$ and small energy interval dE. In the HAS community, the DRC is usually expressed in terms of the surface phonon spectral density, ρ_{zz}, as [29, 30]

$$\frac{dR}{d\Omega dE} \propto \frac{k_f}{|k_{i,z}|}|\tau_{fi}|^2|n(\omega)|e^{-2W(\mathbf{k}_f,\mathbf{k}_i,T)}(\Delta k_z)^2\rho_{zz}, \tag{1}$$

where we have introduced the momentum-transfer vector $\Delta\mathbf{k} = \mathbf{k}_f - \mathbf{k}_i$, and the indices i and f represent the states of the helium atom before and after the scattering event, respectively. The exponential is the Debye-Waller factor, and τ_{fi} is the form factor of the interaction potential between the helium atom and the 2D-silica. In the glass community it is, however, more common to express the above equation in terms of the dynamical structure factor, $S(\Delta\mathbf{k},\omega)$. We, therefore, rewrite our equation as [67]

$$\frac{dR}{d\Omega dE} \propto \frac{k_f}{|k_{i,z}|}|\tau_{fi}|^2 S(\Delta\mathbf{k},\omega), \tag{2}$$

The structure factor is proportional to the surface spectral function of the 2D silica, $\Im D(\Delta\mathbf{k},\omega)$ [68, Appendix N], which, in turn,

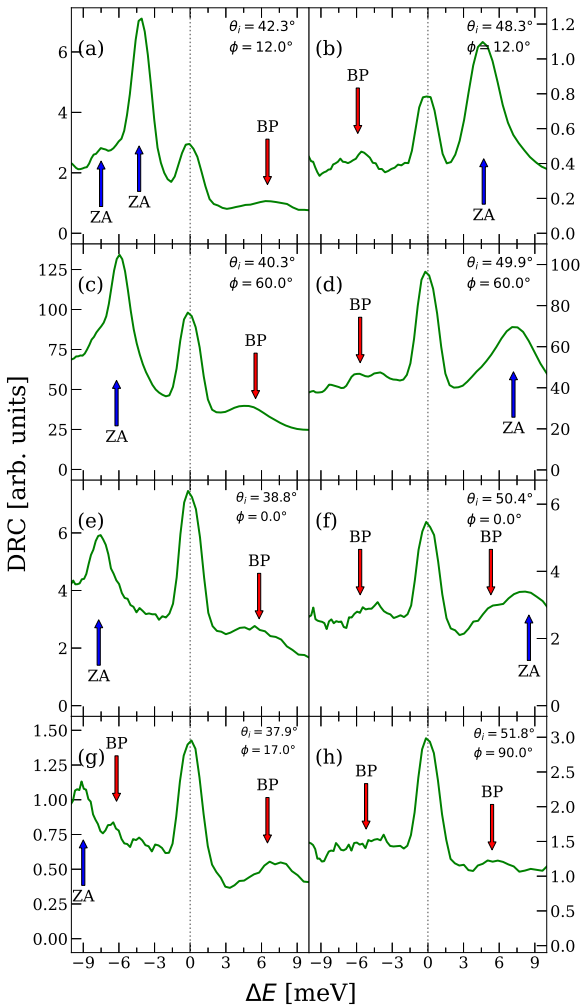

Fig. 1 Several examples of helium atom scattering TOF spectra, converted to energy transfer ΔE, for 2D silica supported on Ru(0001). The incident polar angle relative to the sample normal is θ_i, and ϕ is the azimuthal angle of the sample relative to the principal axis of the Ru(0001). The upward-pointing blue arrows indicate the ZA mode, and the downward-pointing red arrows indicate the BP.

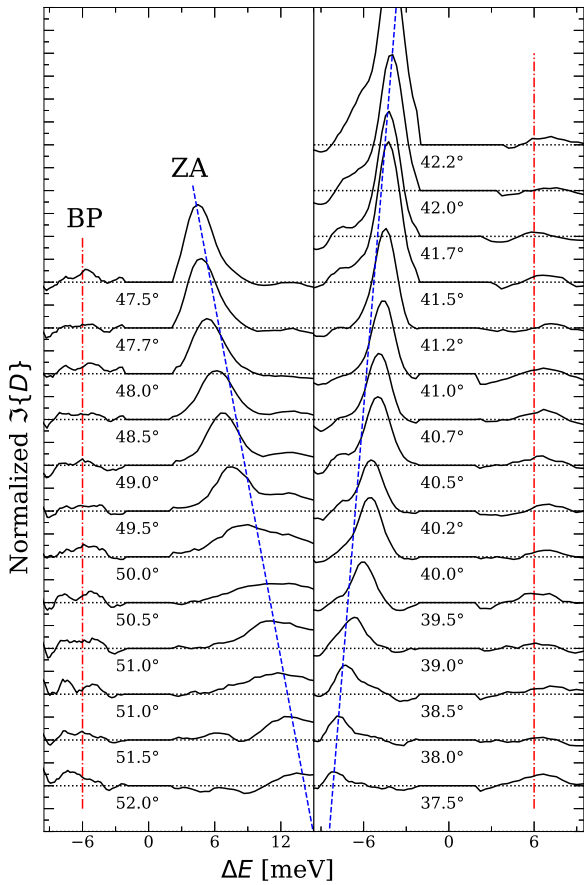

Fig. 2 The spectral function normalized to the linear ω increase as a function of ΔE. The individual spectra shown are a selection taken from those points exhibited in Fig. 4 (a), covering incident polar angles larger than specular (left side) and smaller than specular (right side). The region in the neighbourhood of the strong elastic peak at $\Delta E = 0$ has been subtracted away. Incident angles very close to specular at $\theta_i = 45°$ are not shown because the very intense ZA mode hides the BP. The blue dashed curve marks the dispersive ZA mode and the vertical red dash-dotted lines mark the BP positions, which always remain at the same energy.

is equivalent to the spectral density, $\rho_{zz} = \Im D(\Delta\mathbf{k}, \omega)$.

Figure 2 shows examples of spectral function spectra that have been normalized against the linear frequency dependence (see Methods section, Data Analysis), and Fig. 3, shows the averages of these spectra. The spectra are taken from points on the dispersion curves shown in Fig. 4 (a) for a sample azimuth of 12° relative to the high symmetry direction of the Ru(0001) substrate and incident polar angles ranging from $\theta_i = 37.5°$ to 52°. In each spectrum of Fig. 2, the region close to the large elastic peak at $\Delta E = 0$ has been subtracted. The dashed blue curve marks the ZA mode. It disperses to higher energy values as the incident angle moves further away from the specular position, corresponding to larger values of $|\Delta K|$. The BP appears at the same energy of about 6 meV (corresponding to mode annihilation) on the right side of Fig. 2 and about -6 meV on the left (creation). The BP is denoted by a vertical red dash-dotted line for all conditions and has a FWHM of about 3.5 meV. The averages on

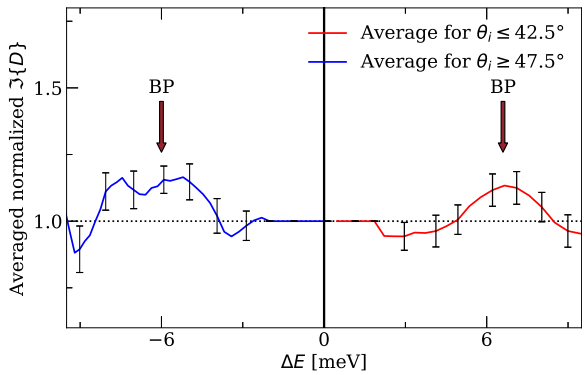

Fig. 3 Left: Average negative ΔE-part of the spectral function in the left hand column of Fig. 2. Right: Average positive ΔE-part of the spectral function in the right hand column of Fig. 2. Error bars are one standard deviation of the average. The reference line at unity is drawn as a guide to the eye. The BP feature, indicated with arrow annotations, as well as its error bars, is situated above the reference.

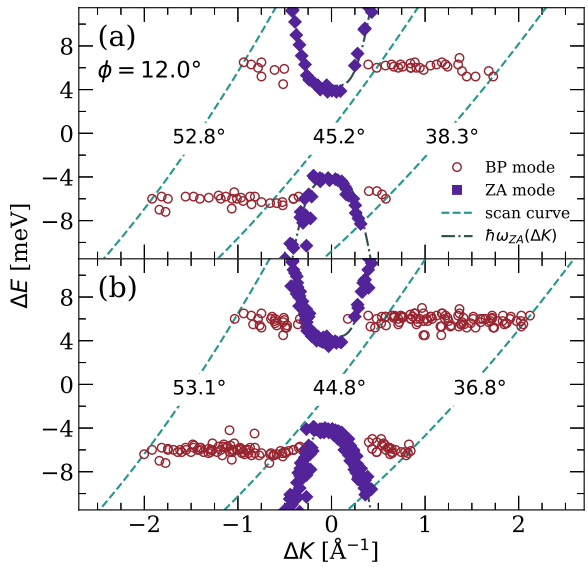

Fig. 4 Phonon dispersion curves showing energy transfer ΔE as a function of parallel momentum transfer ΔK. (a) Dispersion curve for all polar angles θ_i measured at the single azimuthal angle $\phi = 12°$. The BP is shown as red circle data points and the ZA mode as blue diamonds. The dotted green lines show the scan curves for three selected θ_i as indicated. (b) Dispersion curves, including all polar and azimuthal angles measured.

the left-hand side of Fig. 3 correspond to the negative energy exchange region in the left column of Fig. 2, and similarly, the average on the positive energy side in Fig. 3 corresponds to the positive energy values in the right-hand column of Fig. 2. The error bars are taken to be one standard deviation. The error bars for the BP are clearly situated above the reference line at unity. A HAS experiment measures only those inelastic features that cross its scan curve, and this explains why, on the right side of Fig. 2, the BP appears only at positive energy transfer.

Figure 4 shows dispersion curves, i.e., plots of ΔE as a function of parallel momentum transfer, ΔK, obtained as the maxima of $S(\Delta k, \omega)$ with $\omega = \Delta E/\hbar$. Figure 4(a) shows measurements for all polar angles taken at a single azimuthal angle of 12°, while Fig. 4(b) shows all features observed at all polar and azimuthal angles of the total 156 spectra data sets. Also shown in each panel of Fig. 4 are three representative scan curves shown as dashed green curves denoted by the corresponding incident polar angle. The scan curves are obtained from conservation of energy and parallel momentum for the largest and smallest incident angles measured, as well as the one most close to the specular position at $\theta_i = 45°$. The importance of the scan curves is that for a given θ_i, only those quantum features (inelastic or elastic) that the scan curves cross can be observed. The red circle data points give the positions of the BP mode, and it is clear that this is at very nearly constant energy for all ΔK, i.e., it is dispersionless as expected [29]. In the vicinity of the ZA mode the BP feature could not be distinguished because it is obscured by the much larger ZA peak.

In view of the mentioned simulational studies, which show irregular displacements and spatially fluctuating elastic constants associated with the BP anomaly [48, 49, 54–56, 58–61], we can expect that in structurally disordered two-dimensional systems, generically, a BP should be observed. This is in accord with our 2D HET model presented here in the Methods section. Our model gives the important insight that the BP in a 2D material should occur at a similar frequency as in the bulk because the relevant elastic parameters of the 2D system should be similar to those in 3D.

Some scans, e.g. the upper left panel of Fig. 1, contain a feature at about twice the energy of the BP with a FWHM about twice as large. This feature could potentially be interpreted as a double excitation of the BP, if the BP itself is understood as a narrow collection of dispersionless modes. This will be a topic for further investigation.

To conclude: we present the first measurements of the BP in a 2D material, 2D silica. We obtain a value of around 6 meV (1.5 THz), in agreement with the BP position in bulk silica. We attribute our observation to in-plane elastic disorder, which couples to the low-frequency ZA mode probed through inelastic He atom scattering. Future work should include (i) measurements of 2D silica grown on other substrates [64] to assess the influence of the substrate binding energy on the BP behaviour, (ii) temperature-dependent measurements to test if the blueshift behaviour observed for the surface BP of bulk silica does also occur in 2D, (iii) measurements of the BP intensity in samples with different degrees of amorphicity, to investigate the possibility of "tuning" the BP feature, (iv) further investigations of the potential double excitation of the BP at higher energies, and the consequences this observation would impose on the theory.

Methods

Experimental

The vitreous 2D silica sample was prepared in UHV on a Ru(0001) substrate at the Fritz-Haber-Institut in Berlin. We used the same sample that is described in Ref. 66. After preparation, the sample was removed from the UHV chamber in Berlin and transported to Bergen. During transport, the sample was exposed to ambient conditions for more than 20 hours. Upon arrival from Berlin, the sample was installed in the argon-vented sample chamber, which was then pumped down. The background pressure was around 1×10^{-9} mbar. A signal could be obtained from the sample without any initial cleaning; however, to ensure maximum intensity before measurements were done, the sample was heated to 675 K for one hour in an oxygen atmosphere ($p_{O_2} = 2.2\times10^{-6}$ mbar). This improved the measured signal. A slight decline in reflected signal could be observed over a period of days. For this reason, the cleaning process was repeated every day before measurements. This restored the original reflectivity. The HAS experiments were carried out in MAGIE, the molecular beam apparatus at the University of Bergen [69, 70]. The neutral helium beam was created by a free-jet expansion from a source reservoir through a 10±0.5 µm diameter nozzle. The central part of the beam was selected by a skimmer, 410±2 µm in diameter, placed 17±0.5 mm in front of the nozzle. All experiments presented here were carried out on a room temperature sample (T = 296±1 K). The source-detector scattering angle was held constant at 90°. The diffraction scans were measured with a room temperature beam corresponding to a beam energy of E_0=64 meV, while for time-of-flight (TOF) measurements, the beam was cooled to an energy of around E_0=29 meV. The stagnation pressure in the source reservoir was p_0=81 bar for all TOF measurements. The incident beam size was around 4 mm in diameter at the sample position. TOF measurements were performed with a pseudorandom chopper [71]. The measurements presented were conducted as six independent series, varying the incident beam angle (polar angle) θ_i at five different azimuthal angles, $\phi \in \{0.0°, 12.0°, 17.0°, 60.0°, 90.0°\}$. In total 156 TOF spectra were obtained. LEED analysis of the sample at the Fritz-Haber-Institute indicated that the sample was primarily vitreous. This is supported by the fact that no crystalline diffraction pattern was observed with HAS [66]. The azimuthal angle was varied in order to ensure that the effects measured were truly isotropic.

The thickness of an atomically thin layer is difficult to define, a problem well-known in the study of single-layer graphene where it is called the Yakobson paradox [72]. STM imaging has suggested a height of 3-5 Å for bilayer silica films on the Ruthenium substrate [62, 73]. Based on DFT calculations and the mechanical measurements of this sample presented in Ref. 66, this sample has been estimated to have a thickness of about 6.1 Å.

Data Analysis

The single-phonon dynamic structure factor, $S(\Delta\mathbf{k},\omega)$, for a solid with harmonic dynamics, is given by

$$S(\Delta\mathbf{k},\omega) = e^{-2W(\mathbf{k}_f,\mathbf{k}_i,T)} \sum_{i=1}^{n} S^{(\nu)}(\Delta\mathbf{k},\omega), \quad (3)$$

where the index ν in $S^{(\nu)}(\Delta\mathbf{k},\omega)$ runs over the νth-phonon structure factors; one-phonon, two-phonon, and so on. To good approximation, the structure factor of the inelastic HAS data is dominated by the one-phonon contribution. The one-phonon structure factor is by the fluctuation-dissipation theorem related to the strain-strain

response function [74],

$$\chi(\Delta\mathbf{k},\omega) = \chi'(\Delta\mathbf{k},\omega) + i\chi''(\Delta\mathbf{k},\omega) \quad (4)$$
$$= (\Delta k)^2 D(\Delta\mathbf{k},\omega),$$

where $D(\Delta\mathbf{k},\omega) = D' + iD''$ is the response function (Green's function) of the out-of-plane displacements. The dynamic structure factor is therefore given by

$$S^{(1)}(\Delta\mathbf{k},\omega) = |n(\omega)|\chi''(\Delta\mathbf{k},\omega) \quad (5)$$
$$= |n(\omega)|(\Delta k)^2 D''(\Delta\mathbf{k},\omega)$$

Therefore, through the experimentally measured DRC, we have access to the imaginary part of the Green's function, via

$$\frac{dR}{d\Omega dE} \propto \frac{k_f}{|k_{i,z}|}|\tau_{fi}|^2|n(\omega)|e^{-2W(T)}(\Delta\mathbf{k})^2 D''(\Delta\mathbf{k},\omega). \quad (6)$$

Rearranged, this gives

$$D''(\Delta\mathbf{k},\omega) \propto \frac{\frac{dR}{d\Omega dE}|k_{i,z}|}{k_f(\Delta\mathbf{k})^2|n(\omega)||\tau_{f,i}|^2\exp\left[-2W(T)\right]}. \quad (7)$$

The Debye-Waller factor has been introduced as $\exp\left[-2W(\mathbf{k}_f,\mathbf{k}_i,T)\right]$, and the Bose-Einstein function as $n(\omega) = (e^{\beta\hbar\omega}-1)^{-1}$, where $\beta \equiv (k_B T)^{-1}$, k_B is Boltzmann's constant, and T is the sample temperature. The absolute value sign around $n(\omega)$ signifies evaluating it as $n(\omega)+1$ in creation events and $n(\omega)$ for annihilation events. The intensity of the raw data is observed to increase linearly with ω, as expected for the background produced by the low-frequency acoustic phonon modes of a semi-infinite substrate, mediated by the electron density. We, therefore, present the normalized spectral function D'' as D''/ω.

The ZA mode of a thin film on a substrate has a well-understood dispersion relation given by [75]

$$\omega_{\mathrm{ZA}}^2 = \frac{\kappa}{\rho_{2D}}(\Delta k)^4 + \omega_0^2, \quad (8)$$

where κ is the bending rigidity and ρ_{2D} is the 2D mass density. The gap, $\omega_0^2 = g/\rho_{2D}$, is proportional to the elastic coupling strength between the 2D silica and the substrate, g [75]. The form factor τ_{fi} is approximated using the well-known Morse potential matrix elements, i.e., the distorted wave

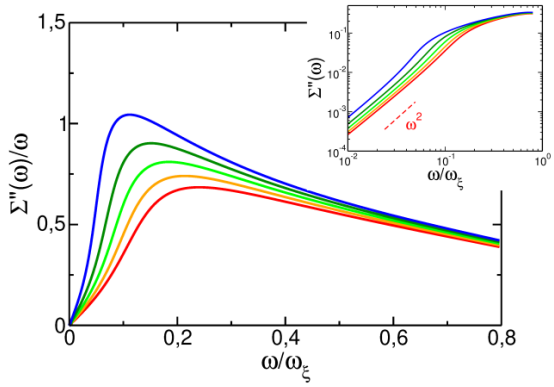

Fig. 5 $\Sigma''(\omega)/\omega$ vs. ω/ω_ξ with $\omega_\xi = [G_0/\rho_m]^{1/2}q_\xi$ and $\gamma = \langle(\Delta G)^2\rangle/G_0^2$ for values $\gamma = 0.35$ to 0.39 (from bottom to top). Inset: $\Sigma''(\omega)$ for the same parameters. The dashed line indicates the low-frequency ω^2 behaviour.

matrix elements of the Morse potential taken with respect to its own eigenstates [76, Ch. 8]. The argument of the Debye-Waller factor, $2W(T)$, within the harmonic lattice approximation and for sufficiently large temperatures is linear in T. It is usually determined by measuring the temperature dependence of the specular diffraction peak. In the present set of experiments, the temperature dependence of the specular peak intensity was not measured, so the argument was taken to be represented by $2W = (\Delta\mathbf{k}^2 C + D)T$ where the coefficients C and D were taken as fitting parameters. The coefficient D is proportional to the so-called Beeby correction, in which the attractive well depth of the interaction potential is added to the energy of normal motion of the He atom [77]. As a check on this procedure, previous data from which the BP was determined at a silica surface [29] were re-examined using this method, and nearly identical results were found for both the Debye-Waller factors and the surface BP intensities.

Theoretical

2-dimensional heterogeneous elasticity theory (HET)

We consider a 2-dimensional system with spatially fluctuating shear modulus $G(\mathbf{r}) = G_0 + \Delta G(\mathbf{r})$, where G_0 is the mean and $\Delta G(\mathbf{r})$ are the fluctuations. In two dimensions the longitudinal and transverse Green's functions (response functions

of the in-plane displacements) are given by

$$D_{L,T}(q,\omega) = \frac{1}{-\omega^2 - i\epsilon + q^2 v_{L,T}(\omega)^2} \tag{9}$$

As usual, one has to add an infinitely small positive real number to the spectral variable ω^2. $v_{L,T}(\omega)$ are effective, complex, frequency-dependent sound velocities, related to a complex, frequency-dependent shear modulus:

$$\begin{aligned} \rho_{2D} v_T(\omega)^2 &= G_0 - \Sigma(\omega) \equiv G(\omega) \\ \rho_{2D} v_L(\omega)^2 &= K + G(\omega), \end{aligned} \tag{10}$$

where K is the bulk modulus. In the self-consistent born approximation (HET-SCBA), the equation for the self energy $\Sigma(\omega)$ is [9]

$$\Sigma(\omega) = \frac{1}{2}\gamma \left(\tfrac{1}{2\pi}\right)^2 \int\limits_{|\mathbf{q}|<q_\xi} d^2q q^2 \Big(D_L(q,\omega) + D_T(q,\omega) \Big) \tag{11}$$

where $\gamma \propto \langle \Delta G^2 \rangle$ is the so-called disorder parameter. The upper cutoff q_ξ is inversely proportional to the correlation length ξ of the fluctuations. This equation predicts

$$\Sigma''(\omega) \propto \Gamma(\omega)/\omega \propto \omega^2 \quad \text{for} \quad \omega < \omega_{BP}$$

where Γ is the the Brillouin line width, and ω_{BP} is the boson peak frequency.

In Fig. 5 we have plotted $\Sigma''(\omega)/\omega$ vs. ω, in which representation the boson peak (which is actually a shoulder in the spectrum, see the inset) becomes visible.

Coupling to the out-of-plane vibrational degrees of freedom

The unperturbed Green's function of the ZA modes is given by [75], $k \equiv |\Delta\mathbf{k}|$:

$$\begin{aligned} D^{(0)}_{ZA}(k,\omega) &= \frac{1}{-\omega^2 - i\epsilon + \omega^2_{ZA}(k)} \\ &= \frac{1}{-\omega^2 - i\epsilon + \omega_0^2 + \frac{1}{\rho_{2D}}\kappa k^4} \end{aligned} \tag{12}$$

The bending (flexural) rigidity κ is given by the layer thickness h, Poisson's ratio ν and Young's modulus of the three-dimensional material $Y_{3D} = 2G_{3D}(1+\nu)$ as

$$\kappa = \frac{h^3}{12(1-\nu^2)} Y_{3D} = \frac{h^3}{6(1-\nu)} G_{3D} \tag{13}$$

G_{3D} is the 3D shear modulus, which obeys

$$G_{3D} = G_{2D}\frac{\rho_{3D}}{\rho_{2D}} = G_{2D}/h\,, \tag{14}$$

from which follows

$$\kappa = \frac{h^2}{6(1-\nu)} G_{2D} \tag{15}$$

This establishes the coupling of the ZA mode to the $2D$ shear elasticity. In the model of two-dimensional heterogeneous elasticity, introduced in the previous paragraph, the boson peak is produced by the frequency dependence of the $2D$ shear modulus $G(\omega)$. This will give rise to a corresponding frequency dependence of the bending rigidity of the ZA modes, i.e. we have to replace the $2D$ shear modulus in Eq. (15) by the frequency-dependent one, given by Eq. (10). The effective complex and frequency-dependent flexural stiffness, which provides the coupling of the ZA modes to the in-plane boson peak, is given by

$$\kappa(\omega) = \frac{h^2}{6(1-\nu)} G_{2D}(\omega) = \frac{h^2}{6(1-\nu)} \big(G_0 - \Sigma(\omega)\big) \tag{16}$$

so that we may write

$$D_{ZA}(k,\omega) = \frac{1}{-\omega^2 + i\epsilon + \omega^2_{ZA}(k) - \Pi(k,\omega)} \tag{17}$$

with

$$\Pi(k,\omega) = V(k)\Sigma(\omega) \tag{18}$$

and the vertex function

$$V(k) = \frac{1}{G_0}\Big(\omega^2_{ZA}(k) - \omega_0^2\Big) \tag{19}$$

In other words: The in-plane disorder-induced anomalous elasticity – with its $2D$ boson peak – is coupled to the flexural out-of-plane degrees of freedom in the same way as the shear modulus to the bending rigidity [75].

For the spectral function, we finally get

$$\chi''(k,\omega) \propto \frac{k^2 V(k)\Sigma''(\omega)}{\left[\omega_{ZA}^2(k) - \Pi'(k,\omega)\right]^2 + \Pi''(k,\omega)^2} \tag{20}$$

The spectral function is proportional to $\Sigma''(\omega)$, i.e. the spectral function, divided by ω, exhibits a boson peak as in Fig. 5.

Data Availability

The experimental datasets will be made available at the repository for open research data at the University of Bergen upon publication. The repository can be accessed at https://dataverse.no/dataverse/uib.

Acknowledgements

Special thanks go to Hans-Joachim Freund and Markus Heyde for making the 2D silica sample available for these experiments. We thank Wolfram Steurer for useful discussions and acknowledge the valuable contributions and stimulating discussions with Gianfranco Pacchioni. B. H. acknowledges funding from the Research Council of Norway (Projects No. 213453 and No. 234159), both within the FRIPRO program. M. T. acknowledges funding from the Research Council of Norway (Project No. 324183), Travel support.

Author Contributions

C. B. prepared the sample, S. D. E. performed the experiments, and M. T. did the data analysis. L. W. and W. S. provided the theoretical model. I. S. and J. R. M. supported the analysis. B. H. designed the experiments. M. T., J. R. M., and B. H. wrote the paper with contributions from all authors.

Competing Interests

The authors declare no competing interests. Data in [78]

References

[1] Debye, P.: Zur Theorie der spezifischen Wärme. Annalen der Physik **344**(14), 789–839 (1912). https://doi.org/10.1002/andp.19123441404

[2] Malinovsky, V.K., Sokolov, A.P.: The nature of boson peak in Raman scattering in glasses. Solid State Communications **57**(9), 757–761 (1986). https://doi.org/10.1016/0038-1098(86)90854-9

[3] Buchenau, U., Prager, M., Nücker, N., Dianoux, A.J., Ahmad, N., Phillips, W.A.: Low-frequency modes in vitreous silica. Phys. Rev. B **34**, 5665–5673 (1986). https://doi.org/10.1103/PhysRevB.34.5665

[4] Chumakov, A.I., Sergueev, I., van Bürck, U., Schirmacher, W., Asthalter, T., Rüffer, R., Leupold, O., Petry, W.: Collective nature of the boson peak and universal transboson dynamics of glasses. Phys. Rev. Lett. **92**, 245508 (2004). https://doi.org/10.1103/PhysRevLett.92.245508

[5] Elliott, S.R.: A unified model for the low-energy vibrational behaviour of amorphous solids. Europhys. Lett. **19**, 201 (1992)

[6] Buchenau, U.: Amorphous materials: Low-frequency vibrations. In: Encyclopedia of Materials: Science and Technology, pp. 212–215. Elsevier, Oxford (2001). https://doi.org/10.1016/b0-08-043152-6/00045-0. https://doi.org/10.1016/b0-08-043152-6/00045-0

[7] Pohl, R.O.: Amorphous materials: Heat capacity. In: Encyclopedia of Materials: Science and Technology, pp. 194–197. Elsevier, Oxford (2001). https://doi.org/10.1016/b0-08-043152-6/00041-3. https://doi.org/10.1016/b0-08-043152-6/00041-3

[8] Zeller, R.C., Pohl, R.O.: Thermal conductivity and specific heat of noncrystalline solids. Phys. Rev. B **4**, 2029–2041 (1971). https://doi.org/10.1103/PhysRevB.4.2029

[9] Schirmacher, W.: Thermal conductivity of glassy materials and the "boson peak". Europhysics Letters (EPL) **73**(6), 892–898 (2006). https://doi.org/10.1209/epl/i2005-10471-9

[10] Beltukov, Y.M., Parshin, D.A., Giordano, V.M., Tanguy, A.: Propagative and diffusive regimes of acoustic damping in bulk amorphous material. Phys. Rev. E **98**, 023005 (2018). https://doi.org/10.1103/PhysRevE.98.023005

[11] Jäckle, J.: In: Phillips, W.A. (ed.) Amorphous Solids: Low-Temperature Properties, p. 135. Springer, Berlin (1981)

[12] Duval, E., Boukenter, A., Achibat, T.: Vibrational dynamics and the structure of glasses. J. Phys. Condens. Matter **2**, 10227 (1990)

[13] Kabeya, M., Mori, T., Fujii, Y., Koreeda, A., Lee, B.W., Ko, J.-H., Kojima, S.: Boson peak dynamics of glassy glucose studied by integrated terahertz-band spectroscopy. Phys. Rev. B **94**, 224204 (2016). https://doi.org/10.1103/PhysRevB.94.224204

[14] Baldi, G., Giordano, V.M., Monaco, G.: Elastic anomalies at terahertz frequencies and excess density of vibrational states in silica glass. Phys. Rev. B **83**, 174203 (2011)

[15] Schroeder, J., Lee, M., Saha, S.K., Persans, P.D.: Raman scattering in glasses at high temperature: the boson peak and structural relaxation kinetics in glasses. Journal of Non-Crystalline Solids **222**, 342–347 (1997). https://doi.org/10.1016/s0022-3093(97)90134-4

[16] Hutt, K.W., Phillips, W.A., Butcher, R.J.: Far-infrared properties of dilute hydroxyl groups in an amorphous silica matrix. Journal of Physics: Condensed Matter **1**(29), 4767–4772 (1989). https://doi.org/10.1088/0953-8984/1/29/003

[17] Ohsaka, T., Ihara, T.: Far-infrared study of low-frequency vibrational states in as_2s_3 glass. Phys. Rev. B **50**, 9569–9572 (1994). https://doi.org/10.1103/PhysRevB.50.9569

[18] Benassi, P., Krisch, M., Masciovecchio, C., Mazzacurati, V., Monaco, G., Ruocco, G., Sette, F., Verbeni, R.: Evidence of high frequency propagating modes in vitreous silica. Phys. Rev. Lett. **77**, 3835–3838 (1996). https://doi.org/10.1103/PhysRevLett.77.3835

[19] Buchenau, U., Nücker, N., Dianoux, A.J.: Neutron scattering study of the low-frequency vibrations in vitreous silica. Phys. Rev. Lett. **53**, 2316 (1984)

[20] Wischnewski, A., Buchenau, U., Dianoux, A.J., Kamitakahara, W.A., Zarestky, J.L.: Neutron scattering analysis of low-frequency modes in silica. Philosophical Magazine B **77**(2), 579–589 (1998). https://doi.org/10.1080/13642819808204986

[21] Buchenau, U.: Neutron scattering investigations of the boson peak. Condensed Matter Physics **22**(4), 43601 (2019). https://doi.org/10.5488/cmp.22.43601

[22] Mori, T., Jiang, Y., Fujii, Y., Kitani, S., Mizuno, H., Koreeda, A., Motoji, L., Tokoro, H., Shiraki, K., Yamamoto, Y., Kojima, S.: Detection of boson peak and fractal dynamics of disordered systems using terahertz spectroscopy. Phys. Rev. E **102**, 022502 (2020). https://doi.org/10.1103/PhysRevE.102.022502

[23] Tomoshige, N., Mizuno, H., Mori, T., Kim, K., Matubayasi, N.: Boson peak, elasticity, and glass transition temperature in polymer glasses: Effects of the rigidity of chain bending. Scientific Reports **9**(1) (2019). https://doi.org/10.1038/s41598-019-55564-2

[24] White, G.K., Collocott, S.J., Cook, J.S.: Thermal expansion and heat capacity of vitreous B_2O_3. Phys. Rev. B **29**, 4778–4781 (1984). https://doi.org/10.1103/PhysRevB.29.4778

[25] Fultz, B., Ahn, C.C., Alp, E.E., Stuhrhahn, W., Toellner, T.S.: Phonons in nanocrystalline ^{57}Fe. Phys. Rev. Lett. **79**, 937 (1997)

[26] Kara, A., Rahman, R.S.: Vibrational properties of metallic nanocrystals. Phys. Rev. Lett. **81**, 1453 (1998)

[27] Perlich, J., Rubeck, J., Botta, S., Gehrke, R., Roth, S.V., Ruderer, M.A., Prams, S.M., Rawolle, M., Zhong, Q., Körstgens, V., Müller-Buschbaum, P.: Grazing incidence wide angle x-ray scattering at the wiggler

beamline BW4 of HASYLAB. Review of Scientific Instruments **81**(10), 105105 (2010). https://doi.org/10.1063/1.3488459

[28] Müller-Buschbaum, P.: Grazing incidence small-angle neutron scattering: challenges and possibilities. Polymer Journal **45**(1), 34–42 (2012). https://doi.org/10.1038/pj.2012.190

[29] Steurer, W., Apfolter, A., Koch, M., Ernst, W.E., Holst, B., Søndergård, E., Manson, J.R.: Observation of the boson peak at the surface of vitreous silica. Phys. Rev. Lett. **99**, 035503 (2007). https://doi.org/10.1103/PhysRevLett.99.035503

[30] Steurer, W., Apfolter, A., Koch, M., Ernst, W.E., Søndergård, E., Manson, J.R., Holst, B.: Surface dynamics measurements of silica glass. Phys. Rev. B **78**, 045427 (2008). https://doi.org/10.1103/PhysRevB.78.045427

[31] Steurer, W., Apfolter, A., Koch, M., Ernst, W.E., Søndergård, E., Manson, J.R., Holst, B.: Anomalous phonon behavior: Blueshift of the surface boson peak in silica glass with increasing temperature. Phys. Rev. Lett. **100**, 135504 (2008). https://doi.org/10.1103/PhysRevLett.100.135504

[32] Steurer, W., Apfolter, A., Koch, M., Ernst, W.E., Søndergård, E., Manson, J.R., B: Vibrational excitations of glass observed using helium atom scattering. Journal of Physics: Condensed Matter **20**(22), 224003 (2008). https://doi.org/10.1088/0953-8984/20/22/224003

[33] Alderwick, A.R., Jardine, A.P., Allison, W., Ellis, J.: An evaluation of the kinematic approximation in helium atom scattering using wavepacket calculations. Surface Science **678**, 65–71 (2018). https://doi.org/10.1016/j.susc.2018.04.019

[34] Holst, B., Alexandrowicz, G., Avidor, N., Benedek, G., Bracco, G., Ernst, W.E., Farías, D., Jardine, A.P., Lefmann, K., Manson, J.R., Marquardt, R., Artés, S.M., Sibener, S.J., Wells, J.W., Tamtögl, A., Allison, W.: Material properties particularly suited to be measured with helium scattering: selected examples from 2D materials, van der Waals heterostructures, glassy materials, catalytic substrates, topological insulators and superconducting radio frequency materials. Physical Chemistry Chemical Physics **23**(13), 7653–7672 (2021). https://doi.org/10.1039/d0cp05833e

[35] Chen, K., Ellenbroek, W.G., Zhang, Z., Chen, D.T.N., Yunker, P.J., Henkes, S., Brito, C., Dauchot, O., van Saarloos, W., Liu, A.J., Yodh, A.G.: Low-frequency vibrations of soft colloidal glasses. Phys. Rev. Lett. **105**, 025501 (2010)

[36] Zhang, L., Zheng, J., Wang, Y., Zhang, L., Jin, Z., Hong, L., Wang, Y., Zhang, J.: Experimental studies of vibrational modes in a two-dimensional amorphous solid. Nature Communications **8**(1) (2017). https://doi.org/10.1038/s41467-017-00106-5

[37] Wang, Y., Hong, L., Wang, Y., Schirmacher, W., Zhang, J.: Disentangling boson peaks and van-Hove singularities in a model glass. Phys. Rev. B **98**, 174207 (2018). https://doi.org/10.1103/PhysRevB.98.174207

[38] Cortie, D.L., Cyster, M.J., Ablott, T.A., Richardson, C., Smith, J.S., Iles, G.N., Wang, X.L., Mitchell, D.R.G., Mole, R.A., de Souza, N.R., Yu, D.H., Cole, J.H.: Boson peak in ultrathin alumina layers investigated with neutron spectroscopy. Phys. Rev. Res. **2**, 023320 (2020). https://doi.org/10.1103/PhysRevResearch.2.023320

[39] Karpov, V.G., Klinger, M.I., Ignat'ev, F.N.: Theory of the low-temperature anomalies in the thermal properties of amorphous structure. Zh. Eksp. Teor. Fiz. **84** (1983)

[40] Buchenau, U., Galperin, Y.M., Gurevich, V.L., Schober, H.R.: Anharmonic potentials and vibrational localization in glasses. Phys. Rev. B **43**, 5039–5045 (1991). https://doi.org/10.1103/PhysRevB.43.5039

[41] Buchenau, U., Galperin, Y.M., Gurevich, V.L., Parshin, D.A., Ramos, M.A., Schober, H.R.: Interaction of soft modes and sound

waves in glasses. Phys. Rev. B **46**, 2798–2808 (1992). https://doi.org/10.1103/PhysRevB.46.2798

[42] Parshin, D.A.: Soft potential model and universal properties of glasses. Physica Scripta **T49A**, 180–185 (1993). https://doi.org/10.1088/0031-8949/1993/t49a/030

[43] Guillot, B., Guissani, Y.: Boson peak and high frequency modes in amorphous silica. Phys. Rev. Lett. **78**, 2401–2404 (1997). https://doi.org/10.1103/PhysRevLett.78.2401

[44] Horbach, J., Kob, W., Binder, K.: High frequency sound and the boson peak in amorphous silica. The European Physical Journal B **19**(4), 531–543 (2001). https://doi.org/10.1007/s100510170299

[45] Wang, C., Tamai, Y., Kuzuu, N.: A molecular dynamics study on vibration spectra of a-SiO_2 surface. Journal of Non-Crystalline Solids **321**(3), 204–209 (2003). https://doi.org/10.1016/s0022-3093(03)00233-3

[46] Maurer, C., Schirmacher, W.: Local oscillators vs. elastic disorder: a comparison of two models for the boson peak. J. Low-Temp. Phys. **137**, 453 (2004)

[47] Marruzzo, A., Schirmacher, W., Fratalocchi, A., Ruocco, G.: Heterogeneous shear elasticity of glasses: the origin of the boson peak. Scientific Reports **3**(1) (2013). https://doi.org/10.1038/srep01407

[48] Tanguy, A., Wittmer, J.-P., Barrat, J.-L.: Continuum limit of amorphous elastic bodies: A finite-size study of low-frequency harmonic vibrations. Phys. Rev. B **66**, 174205 (2002)

[49] Maloney, C., Lemaître, A.: Universal breakdown of elasticity at the onset of material failure. Phys. Rev. Lett. **93**, 195501 (2004)

[50] Léonforte, F., Tanguy, A., Wittmer, J.P., Barrat, J.-L.: Continuum limit of amorphous elastic bodies ii: Linear response to a point source force. Phys. Rev. B **70**, 014203 (2004)

[51] Léonforte, F., Boissière, R., Tanguy, A., Wittmer, J.P., Barrat, J.-L.: Continuum limit of amorphous elastic bodies iii: Three-dimensional systems. Phys. Rev. B **72**, 224206 (2005)

[52] Léonforte, F., Tanguy, A., Wittmer, J.P., Barrat, J.-L.: Inhomogeneous elastic response of silica glass. Phys. Rev. Lett. **97**, 055501 (2006)

[53] Pan, Z., Benzine, O., Sawamura, S., Limbach, R., Koike, A., Bennett, T.D., Wilde, G., Schirmacher, W., Wondraczek, L.: Disorder classification of the vibrational spectra of modern glasses. Phys. Rev. B **104**, 134106 (2021). https://doi.org/10.1103/PhysRevB.104.134106

[54] Shintani, H., Tanaka, H.: Universal link between the boson peak and transverse phonons in glass. Nature Materials **7**, 879 (2008)

[55] Beltukov, Y.M., Fusco, C., Parshin, D.A., Tanguy, A.: Theory of sparse random matrices and vibrational spectra of amorphous solids. Phys. Rev. E **93**, 023006 (2016)

[56] Hu, Y.-C., Tanaka, H.: Origin of the boson peak in amorphous solids. Nature Physics **18**, 669–677 (2022)

[57] Schirmacher, W., Diezemann, G., Ganter, C.: Harmonic vibrational excitations in disordered solids and the boson peak. Phys. Rev. Lett. **81**, 136 (1998)

[58] Beltukov, Y.M., Parshin, D.A.: Theory of sparse random matrices and vibrational spectra of amorphous solids. Phys. Sol. State. **53**, 151 (2011)

[59] Conyuh, D.A., Beltukov, Y.M., Parshin, D.A.: Boson peak in two-dimensional random matrix models. J. Phys. Conf. Ser. **929**, 012031 (2017)

[60] Conyuh, D.A., Beltukov, Y.M.: Random matrix theory and the boson peak in two-dimensional systems. Phys. Solid State **62**(4), 689–695 (2020)

[61] Raikov, I.O., Conyuh, D.A., Ipatov, A.N., Parshin, D.A.: Boson peak in amorphous graphene in the stable random matrix model. Physics of the Solid State **62**(11), 2143–2153 (2020). https://doi.org/10.1134/s1063783420110232

[62] Büchner, C., Wang, Z.-J., Burson, K.M., Willinger, M.-G., Heyde, M., Schlögl, R., Freund, H.-J.: A large-area transferable wide band gap 2d silicon dioxide layer. ACS Nano **10**(8), 7982–7989 (2016). https://doi.org/10.1021/acsnano.6b03929

[63] Büchner, C., Heyde, M.: Two-dimensional silica opens new perspectives. Progress in Surface Science **92**(4), 341–374 (2017). https://doi.org/10.1016/j.progsurf.2017.09.001

[64] Huang, P.Y., Kurasch, S., Srivastava, A., Skakalova, V., Kotakoski, J., Krasheninnikov, A.V., Hovden, R., Mao, Q., Meyer, J.C., Smet, J., Muller, D.A., Kaiser, U.: Direct imaging of a two-dimensional silica glass on graphene. Nano Letters **12**(2), 1081–1086 (2012). https://doi.org/10.1021/nl204423x

[65] Huang, P.Y., Kurasch, S., Alden, J.S., Shekhawat, A., Alemi, A.A., McEuen, P.L., Sethna, J.P., Kaiser, U., Muller, D.A.: Imaging atomic rearrangements in two-dimensional silica glass: Watching silica's dance. Science **342**(6155), 224–227 (2013). https://doi.org/10.1126/science.1242248

[66] Büchner, C., Eder, S.D., Nesse, T., Kuhness, D., Schlexer, P., Pacchioni, G., Manson, J.R., Heyde, M., Holst, B., Freund, H.-J.: Bending rigidity of 2d silica. Phys. Rev. Lett. **120**, 226101 (2018). https://doi.org/10.1103/PhysRevLett.120.226101

[67] Hofmann, F., Toennies, J.P.: High-resolution helium atom time-of-flight spectroscopy of low-frequency vibrations of adsorbates. Chemical Reviews **96**(4), 1307–1326 (1996). https://doi.org/10.1021/cr9502209

[68] Ashcroft, N.W., Mermin, N.D.: Solid State Physics. Harcourt College Publishers, New York (1976)

[69] Apfolter, A.: Wiederaufbau und Test einer He–Streuapparatur und erste Streuexperimente an amorpher sowie kristalliner SiO_2-Oberfläche. Master's thesis, Graz University of Technology (2005)

[70] Eder, S.D., Samelin, B., Bracco, G., Ansperger, K., Holst, B.: A free jet (supersonic), molecular beam source with automatized, 50 nm precision nozzle-skimmer positioning. Review of Scientific Instruments **84**(9), 093303 (2013). https://doi.org/10.1063/1.4821147

[71] Koleske, D.D., Sibener, S.J.: Generation of pseudorandom sequences for use in cross-correlation modulation. Review of Scientific Instruments **63**(8), 3852–3855 (1992). https://doi.org/10.1063/1.1143282

[72] Huang, Y., Wu, J., Hwang, K.C.: Thickness of graphene and single-wall carbon nanotubes. Phys. Rev. B **74**, 245413 (2006)

[73] Yang, B., Kaden, W.E., Yu, X., Boscoboinik, J.A., Martynova, Y., Lichtenstein, L., Heyde, M., Sterrer, M., Włodarczyk, R., Sierka, M., Sauer, J., Shaikhutdinov, S., Freund, H.-J.: Thin silica films on ru(0001): monolayer, bilayer and three-dimensional networks of [SiO4] tetrahedra. Physical Chemistry Chemical Physics **14**(32), 11344 (2012). https://doi.org/10.1039/c2cp41355h

[74] Schirmacher, W., Scopigno, T., Ruocco, G.: Theory of vibrational anomalies in glasses. Journal of Non-Crystalline Solids **407**, 133–140 (2015)

[75] Amorim, B., Guinea, F.: Flexural mode of graphene on a substrate. Phys. Rev. B **88**, 115418 (2013). https://doi.org/10.1103/PhysRevB.88.115418

[76] Goodman, F.O., Wachman, H.Y.: Quantum theory of gas–surface scattering. In: Dynamics of Gas-Surface Scattering, pp. 143–180. Elsevier, New York (1976). https://doi.org/10.1016/b978-0-12-290450-9.50013-0. https://doi.org/10.1016/b978-0-12-290450-9.50013-0

[77] Beeby, J.L.: The scattering of helium atoms from surfaces. Journal of Physics C: Solid State Physics **4**(18), 359–362 (1971). https://doi.org/10.1088/0022-3719/4/18/001

[78] Holst, B., Eder, S.D., Tømterud, M.: Helium Atom Scattering on Amorphous Bilayer Silica. https://doi.org/10.18710/CMKTQX. https://doi.org/10.18710/CMKTQX